

JPE

# Design of a Novel Integrated L-C-T Used in PSFB ZVS Converter

Jiashen Tian<sup>†</sup>, Junxia Gao<sup>\*</sup> and Yiming Zhang<sup>\*</sup>

<sup>†\*</sup>Faculty of Information, Beijing University of Technology, Beijing, China

## Abstract

To enhance the zero-voltage switching (ZVS) range and power density of the phase-shift full-bridge (PSFB) ZVS converter used in geophysical exploration, an additional resonant inductor used as leakage inductance and a blocking capacitor which is equivalent to interlayer capacitance are integrated into a novel integrated inductor-capacitor-transformer (L-C-T). The leakage inductance and equivalent interlayer capacitance of the novel integrated L-C-T are difficult to determine by conventional methods. To address this issue, this paper presents the accurate and efficient methods to compute the leakage inductance and equivalent interlayer capacitance. Moreover, the accuracy of the methodology which is based on the electromagnetic energy and Lebedev's method is verified by experimental analysis and finite element analysis (FEA). Taking the problem of the novel integrated L-C-T into consideration, the losses of the integrated L-C-T are analyzed and the temperature rise of the integrated L-C-T are determined by FEA. Finally, a PSFB ZVS converter prototype with the novel integrated L-C-T is designed and tested.

**Key words:** ZVS, integrated L-C-T, leakage inductance, equivalent interlayer capacitance, electromagnetic energy, Lebedev.

## I. INTRODUCTION

In soft-switching technology, the switching losses of electronic devices can be reduced, so that the high-power DC-DC converter can achieve high-frequency[1]-[3]. However, the primary windings of a transformer in the soft-switching converter typically requires a series resonant inductor and a blocking capacitor, which increase the size and weight of the transformer[4]-[5]. Through the rational design of the magnetic circuit and structure, the resonant inductor and blocking capacitor can be integrated into the transformer[6]-[8]. The integration of passive devices has become one of the core technologies, which further improve the power density of the DC-DC converter.

The proposed phase-shift full-bridge (PSFB) zero-voltage switching (ZVS) converter, which is applied for electric geological prospecting, is both required to reach ZVS under a light-load and output 40 kW under a heavy-load. Consequently, the integrated L-C-T in the proposed converter should not only have enough stray capacitance to absorb the DC harmonics, but also have enough leakage inductance to

replace the resonant inductor. Various methods of integrating capacitance and leakage inductance into a transformer, which are based on the planar winding and the leakage layer, have been described [9]-[12]. However, as the cross-section of the planar windings is usually perpendicular to the leakage magnetic flux of the transformer, the eddy current effect of the planar windings is clearly enhanced[8]. Furthermore, the planar windings and leakage layers are not suitable for high-power, high-frequency transformers.

To overcome this drawbacks, the novel integrated L-C-T is designed, consisting of copper foil primary windings and separated windings[9]-[12]. At the same times, these parts can ensure the integrity of the primary winding and facilitate the integration of the blocking capacitor. The separated secondary windings of the novel integrated L-C-T are used to increase the leakage inductance. As the structure of the novel integrated L-C-T is complex, it is difficult to determine the leakage inductance and equivalent interlayer capacitance[4]. Additionally, as the resonant inductor and DC blocking capacitor are integrated into the novel integrated L-C-T, the loss density and temperature rise of the integrated components seriously increases.

To address the above problems, the methods based on electric field energy, magnetic field energy and Lebedev's equations are developed to determine the leakage inductance and interlayer capacitance of the proposed integrated L-C-T

are presented in this paper[13]-[15]. In addition, the theoretical analysis is verified by finite element analysis (FEA) and experimental measurement. Furthermore, the loss of the novel integrated L-C-T is analyzed, and the actual operating temperature is calculated by FEA. Finally, the prototype of the novel integrated L-C-T is tested on the proposed PSFB ZVS converter, and its performance is verified.

## II. THE STRUCTURE AND CHARACTERISTICS OF THE NOVEL INTEGRATED L-C-T

The novel integrated L-C-T is used in a PSFB ZVS converter for a geophysical equipment, which provides a high-voltage, high current signal to earth. And the topology of proposed converter is shown in Fig. 1. The conventional transformer plays the roles of power transmitter and voltage converter in the proposed converter. The resonant inductor resonates with the parallel capacitor ( $C_1$ - $C_4$ ) across the insulated-gate bipolar transistors (IGBTs), to ensure the IGBTs achieve ZVS. The circuit configuration of proposed converter is based on the conventional PSFB converter, and  $C_1=C_2$ ,  $C_3=C_4$ ,  $\alpha^2 L_{out} \gg L_{lk}$ , where  $L_{out}$  is output filter inductor,  $L_{lk}$  is the leakage inductance of the novel integrated L-C-T,  $\alpha$  is the turns ratio of the L-C-T. The blocking capacitor  $C_b$  can eliminate the DC bias of the transformer in the novel integrated L-C-T. Through analysis and design, the resonant inductor, blocking capacitor and transformer in the proposed PSFB ZVS converter can be replaced by the novel integrated L-C-T[16]-[20].

The primary windings  $n_{pri}$  are all wound around the center leg, as shown in Fig. 2. The EPCOS dielectric films are applied between the primary windings, while the blocking capacitor can be replaced by the equivalent interlayer capacitance between the primary windings and EPCOS films. The secondary windings are separated into two parts to reduce the voltage stress of the secondary rectifier diodes. Additionally, the secondary windings  $n_{s11}$  and  $n_{s21}$  are wound around the center column, while the secondary windings  $n_{s12}$  and  $n_{s22}$  are wound around the side column. As the primary and secondary windings are not around in the same column, the leakage inductance of the novel integrated L-C-T is sufficient to replace the resonant inductor.

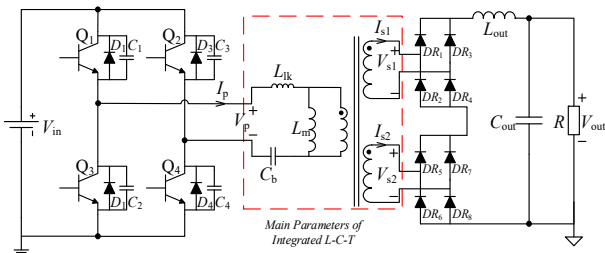


Fig. 1. Main parameters of the PSFB ZVS converter.

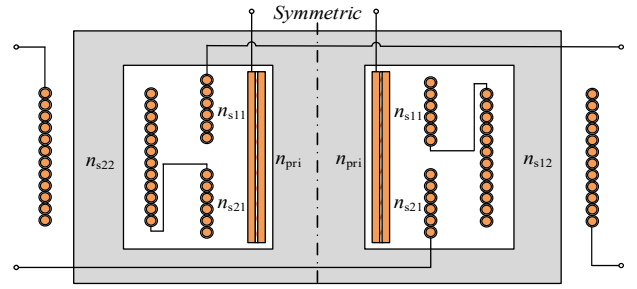


Fig. 2. The main structure of the novel integrated L-C-T.

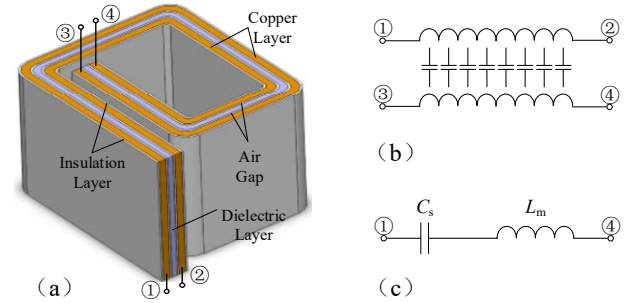


Fig. 3. The structure of the primary winding for the novel integrated L-C-T.

## III. INTEGRATION OF THE BLOCKING CAPACITOR

In order to integrate the blocking capacitor into the primary windings of the transformer, the primary windings of the novel integrated L-C-T are made of the flexible multi-layer. The detailed structure of the proposed primary windings is shown in Fig. 3. As shown in Fig. 3(b), a lumped capacitance can be formed between the two primary layers, particularly considering that the EPCOS dielectric layer is sandwiched between the two primary layers. While terminals 2 and 3 are floating and terminals 1 and 4 are used as the primary windings of the transformer, the stray capacitance  $C_s$  of the primary windings forms a series relation with the excitation inductance  $L_m$ , as shown in Fig. 3(c).

### A. Calculation of static interlayer capacitance

To obtain the equivalent interlayer capacitance  $C_b'$  of the primary windings, it is necessary to calculate the static interlayer capacitance  $C_b$ . The static interlayer capacitance  $C_b$  of the novel integrated L-C-T is composed of capacitances  $C_{ins}$  and  $C_{die}$ , as expressed in equation (1), where the static capacitance  $C_{ins}$  between the insulating layer and copper layer is given by the equation (2), and the static capacitance between the dielectric layer and the copper layer  $C_{die}$  is given by the equation (3). Due to the air gaps between the flexible multi-layer foils, the actual permittivities are different from the permittivities of the dielectric and insulating layers, and the equivalent methods are stated as shown in equations (4) and (5)[21,22].

$$C_b = C_{ins} + C_{die} \quad (1)$$

$$C_{die} = \frac{\varepsilon_0 \varepsilon'_{die} l_{pri} n_{pri} w_{pri}}{t_{die} + 2t_{air}} \quad (2)$$

$$C_{ins} = \frac{\varepsilon_0 \varepsilon'_{ins} l_{pri} n_{pri} w_{pri}}{t_{ins} + 3t_{air}} \quad (3)$$

$$\varepsilon'_{die} = \frac{\varepsilon_{die} \cdot (t_{die} + 2t_{air})}{t_{die} + \varepsilon_{die} \cdot 2t_{air}} \quad (4)$$

$$\varepsilon'_{ins} = \frac{\varepsilon_{ins} \cdot (t_{ins} + 3t_{air})}{t_{ins} + \varepsilon_{ins} \cdot 3t_{air}} \quad (5)$$

where,  $\varepsilon'_{die}$  represents the equivalent permittivity of the dielectric film,  $\varepsilon'_{ins}$  denotes the equivalent permittivity of insulating film,  $\varepsilon_0$  indicates the permittivity of the vacuum,  $l_{pri}$  is the average length of the primary turns,  $n_{pri}$  is the turns of the primary,  $w_{pri}$  is the average width of the foil windings,  $t_{die}$  is the average thickness of the dielectric films,  $t_{ins}$  is the average thickness of the insulating layer,  $t_{air}$  is the equivalent thickness of the air gap.

### B. Calculation of the equivalent interlayer capacitance.

The static interlayer capacitance is related to the winding structure and winding materials, but not to the voltage distribution of windings. Besides, the actual distribution of the charges depends on the voltage distribution of windings. Accordingly, the equivalent interlayer capacitance of the novel integrated L-C-T primary windings is dependent on both the structure and the voltage distribution of winding. The corresponding stored electrostatic energy between the primary layers is given by the following equation:

$$\begin{aligned} W_\varepsilon &= \frac{1}{2} \iiint_V D \cdot E dV \\ &= W_{die} + W_{ins} \\ &= \frac{1}{2} C_{die} V_{Cb}^2 + \frac{1}{2} C_{ins} V_{Cb}^2 \end{aligned} \quad (6)$$

where,  $W_{die}$  is the stored electric energy in the dielectric films,  $W_{ins}$  is the stored electric energy in the insulating films.

To facilitate the calculation, we can assume that the transformer magnetic field distribution is uniform and the voltage in the winding is evenly distributed. As the two plates of  $C_{die}$  belong to the same number of turns, the voltage across  $C_{die}$  is  $V_{Cb}$ . The plates of  $C_{ins}$  belong to the different turns of primary windings, so the voltage across  $C_{ins}$  is  $V_{Cb} + (V_{in} - V_{Cb})/n_{pri}$ . According to the winding structure in Fig 3(a), the electric fields of  $C_{die}$  and  $C_{ins}$  are given by the equation:

$$\begin{cases} E_{die}(x) = \frac{V_{Cb}}{t_{die} + 2t_{air}} \\ E_{ins}(x) = \frac{V_{in} + (n_{pri} - 1)V_{Cb}}{(t_{ins} + 3t_{air}) \cdot n_{pri}} \end{cases} \quad (7)$$

where,  $V_{Cb}$  is the voltage across blocking capacitance,  $V_{in}$  is the input voltage.

Thus,  $W_{die}$  is also given by the equation:

$$\begin{aligned} W_{die} &= \frac{1}{2} \iiint_V \varepsilon_0 \varepsilon'_{die} E_{die}^2(x) dV \\ &= \frac{1}{2} \frac{\varepsilon_0 \varepsilon'_{die} l_{pri} w_{pri} V_{Cb}^2}{(t_{die} + 2t_{air})} \\ &= \frac{1}{2} C'_{die} V_{Cb}^2 \end{aligned} \quad (8)$$

and  $W_{ins}$  is also given by the following equation:

$$\begin{aligned} W_{ins} &= \frac{1}{2} \iiint_V \varepsilon_0 \varepsilon'_{ins} E_{ins}^2(x) dV \\ &= \frac{1}{2} \frac{\varepsilon_0 \varepsilon'_{ins} l_{pri} w_{pri} [V_{in} + (n_{pri} - 1)V_{Cb}]^2}{(t_{ins} + 3t_{air}) \cdot n_{pri}^2} \\ &= \frac{1}{2} C'_{ins} \frac{[V_{in} + (n_{pri} - 1)V_{Cb}]^2}{n_{pri}^2} \\ &= \frac{1}{2} C'_{ins} V_{Cb}^2 \end{aligned} \quad (9)$$

where,  $C'_{ins}$  is the equivalent interlayer capacitance of insulation and  $C'_{die}$  is the equivalent interlayer capacitance of the dielectric.

Based on the stored electric energy, the equivalent interlayer capacitance of the novel integrated L-C-T primary layers can be expressed as follows:

$$\begin{cases} C'_{die} = C_{die} \\ C'_{ins} = \frac{[V_{in} + (n_{pri} - 1)V_{Cb}]^2}{n_{pri}^2 V_{Cb}^2} C_{ins} \end{cases} \quad (10)$$

Assuming that the voltage across blocking capacitance  $V_{Cb} = 0.1V_{in}$ , as previously those described[23], then the equivalent capacitance is as follows:

$$C'_{ins} = \frac{(n_{pri} + 9)^2}{n_{pri}^2} C_{ins} \quad (11)$$

The equivalent interlayer capacitance is expressed as:

$$\begin{aligned} C'_b &= C'_{die} + C'_{ins} \\ &= \frac{\varepsilon_0 \varepsilon'_{die} l_{pri} n_{pri} w_{pri}}{t_{die} + 2t_{air}} + \frac{(n_{pri} + 9)^2}{n_{pri}^2} \cdot \frac{\varepsilon_0 \varepsilon'_{ins} l_{pri} n_{pri} w_{pri}}{t_{ins} + 3t_{air}} \end{aligned} \quad (12)$$

## IV. INTEGRATION OF THE RESONANT INDUCTOR

The novel integrated L-C-T with separated secondary windings is presented in Fig. 2. As the primary and secondary windings are not wound around the same column, the linkage of the windings decreases and the leakage flux increases. The flux distribution of the novel integrated L-C-T is presented in Fig. 4, where  $\Phi_0$ ,  $\Phi_1$  and  $\Phi_2$  are the main fluxes,  $\Phi_{in}$  is the inner leakage flux,  $\Phi_{eq}$  is the equivalent leakage flux and  $\Phi_y$  is the yoke leakage flux. Half of the leakage inductance consists of three components, namely the inner leakage inductance  $L_{in}$ , the yoke leakage inductance  $L_y$ , and the equivalent leakage inductance  $L_{eq}$ . Due to the symmetry of novel integrated L-C-T, the leakage inductance of the novel

integrated L-C-T is expressed as follows:

$$L_{lk} = 2(L_{in} + L_y + L_{cq}) \quad (13)$$

#### A. Calculation of inner leakage inductance

As the novel integrated L-C-T is not designed by the conventional methods, the empirical formula is not suitable for calculating the  $L_{in}$  of the novel integrated L-C-T. In addition, as the prototype is needed to obtain  $L_{in}$  through measurement, the designing process of the novel integrated L-C-T is slowed down. Consequently, the stored magnetic energy is used to determine inner leakage inductance  $L_{in}$ , which is simpler and more accurate than the other methods.

The inner leakage flux density of the half-core window is shown in Fig. 5, where  $H(x)$  is the magnetic flux density of the inner leakage field,  $H(max)$  is the maximum flux density of the inner field,  $H(mid)$  is the middle flux density of the inner field. At stage  $t_1-t_2$ , the flux density increases from zero to  $H(max)$ , because the  $n_{pri}$  are turned around the center leg of core. At stage  $t_2-t_3$ , the flux density is kept at  $H(max)$ , because of the insulation between the primary and secondary windings of the transformer. At stage  $t_3-t_4$ , as some of secondary windings ( $n_{s11}$  and  $n_{s21}$ ) are turned around the center leg of core,  $H(x)$  decreases quickly. At stage  $t_4-t_5$ , the magnetic field remains at  $H(mid)$ , because of the air between the center and side leg of the core. At stage  $t_5-t_6$ ,  $H(x)$  decreases to zero, due to the  $n_{s12}$  being around the side leg of core. According to the principle of magnetic energy, a plenty of energy is stored in the leakage magnetic field at stage  $t_1-t_6$ . And the magnetic energy storage of the inner leakage field increases with the number of  $n_{s12}$ .

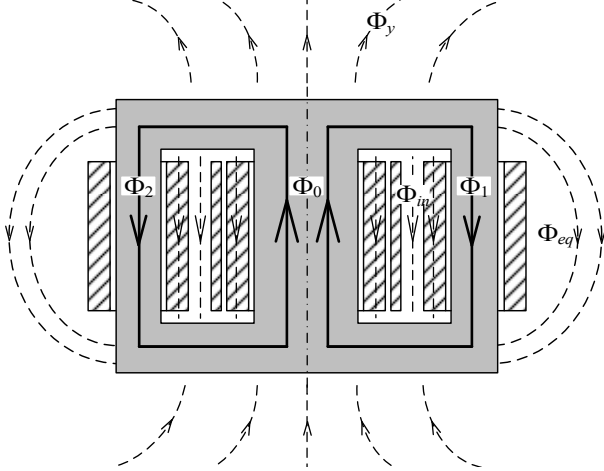


Fig. 4. The flux distribution of the novel integrated L-C-T.

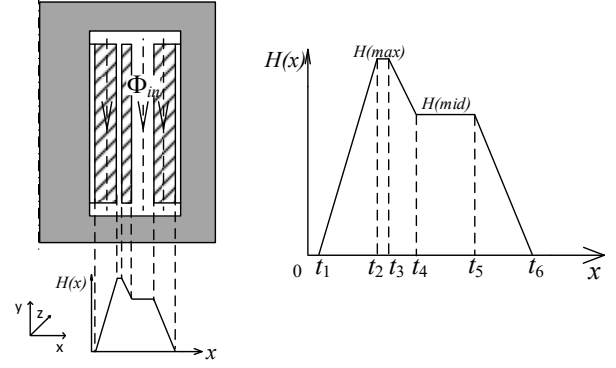


Fig. 5. The inner leakage flux density of the half-core window.

TABLE I  
CALCULATION OF THE STORED MAGNETIC ENERGY IN THE INNER LEAKAGE FIELDS

Internal	The stored energy
$t_1-t_2$	$W_{in\_1} = \frac{1}{2} \mu_0 l_w h_w \int_0^{t_2-t_1} \left[ \frac{n_{pri} I_{pri}}{(t_2-t_1) h_w} x \right]^2 dx$
$t_2-t_3$	$W_{in\_2} = \frac{1}{2} \cdot \frac{\mu_0 l_w n_{pri}^2 I_{pri}^2}{h_w} (t_3-t_2)$
$t_3-t_4$	$W_{in\_3} = \frac{1}{2} \mu_0 l_w h_w \int_0^{t_4-t_3} \left( \frac{n_{pri} I_{pri} - \frac{n_{s11} I_{sec}}{t_4-t_3} x}{h_w} \right)^2 dx$
$t_4-t_5$	$W_{in\_4} = \frac{1}{2} \mu_0 l_w h_w \left( \frac{n_{pri} I_{pri} - n_{s11} I_{sec}}{h_w} \right)^2 (t_5-t_4)$
$t_5-t_6$	$W_{in\_5} = \frac{1}{2} \mu_0 l_w h_w \int_{t_5}^{t_6} \left[ -\frac{\frac{n_{s21} I_{sec}}{t_6-t_5} (x-t_6)}{h_w} \right]^2 dx$

The energy of the inner leakage field  $W_{in}$  can be expressed as follows:

$$W_{in} = \frac{\mu_0}{2} \int H(x)^2 dv \quad (14)$$

As the magnetic field distribution is shown in Fig. 5, the stored magnetic energy  $W_{in}$  can be calculated as follows[12]-[13]:

$$W_{in} = \frac{1}{2} \mu_0 l_w h_w \sum_{i=1}^6 \int_{t_{i-1}}^{t_i} H_i(x)^2 dx \quad (15)$$

where,  $\mu_0$  is the permeability of the vacuum,  $l_w$  is the width of the core window along the z axis,  $h_w$  is the height of the core window.

The stored magnetic energy in each stage of the inner leakage field can be expressed as shown in Table 1, where  $I_{pri}$  is the peak current of the primary windings,  $I_{sec}$  is the peak current of the secondary windings.

In summary, the inner leakage inductance of the novel integrated L-C-T is as follows:

$$L_{in} = \frac{\sum_{a=1}^5 W_{in\_a}}{I_{pri}^2} \quad (16)$$

### B. Calculation of the yoke leakage inductance

The yoke leakage inductance is proportional to the square of the  $n_{s12}$  [15]. As shown in Equation (17), the yoke leakage inductance  $L_{s\_y}$  at the secondary windings is calculated by Lebedev's method[24], then the yoke leakage inductance  $L_y$  at the primary windings can be calculated by Equation (18):

$$L_{s\_y} = \frac{\mu_0 n_{s12}^2 b_c l_w}{6 h_c} \quad (17)$$

$$L_y = \alpha^2 L_{s\_y} \quad (18)$$

where,  $b_c$  is the width of the core along x axis,  $h_c$  is the height of the core,  $\alpha$  is the turns ratio of the novel integrated L-C-T.

### C. Calculation of the equivalent leakage inductance

The equivalent leakage inductance of the secondary  $L_{s\_eq}$  is related to the turns of  $n_{s12}$ , the average length  $l_{s12}$  of  $n_{s12}$ , the width of the core window along the x axis  $b_w$  and the height of the core window  $h_w$ [25]. Also, while the core structure is determined, the equivalent leakage inductance  $L_{eq}$  is only proportional to the square of  $n_{s12}$ . Consequently,  $L_{s\_eq}$  is converted to the primary to get  $L_{eq}$ . As is shown in the following equations:

$$L_{s\_eq} = \frac{\mu_0 n_{s12}^2 l_{s12} b_w}{3 h_w} \quad (19)$$

$$L_{eq} = \alpha^2 L_{s\_eq} \quad (20)$$

Based on the stored magnetic energy method and Lebedev's method, the leakage inductance of the novel integrated L-C-T can be calculated using Equation (13). The proposed methods are more suitable for the integrated L-C-T with complex structure.

## V. LOSSES OF NOVEL INTEGRATED L-C-T

As the blocking capacitor, the resonant inductor and the transformer are integrated into the novel integrated L-C-T, the size and weight of the proposed devices are reduced. In contrast, the loss density and the temperature of the novel integrated L-C-T are increased. To solve the overheating problem of the integrated components, the losses of these components are analyzed in paper. Considering the serious overheating of the novel integrated L-C-T, the necessary cooling measures are adopted. The thermal design is one of the most important parts for the novel integrated L-C-T, and the losses of the proposed L-C-T are discussed in parts A-C.

### A. Dielectric losses

$$P_{Cb} = 2\pi f \cdot C_b' \cdot V_{Cb}^2 \cdot \tan \delta \quad (21)$$

The dielectric loss of the equivalent capacitance is

associated with the following factors: the operating frequency  $f$ , the voltage across capacitor  $V_{Cb}$ , the equivalent capacitance of primary  $C_b'$  and the small-signal loss factor ( $\tan \delta$ ). The  $\tan \delta$  of the dielectric is known by measurement at 20 kHz.

### B. Core losses

The core losses of the transformer include hysteresis loss, anomalous eddy current loss and eddy current loss. The core losses in the full-bridge circuit are expressed as follows:

$$\begin{aligned} P_{Fe} &= P_h + P_a + P_e \\ &= P_h + k_a B_m^{1.5} f^{1.5} + k_e B_m^2 f^2 \end{aligned} \quad (22)$$

where,  $P_h$  denotes the hysteresis loss,  $P_a$  represents the anomalous eddy current loss,  $P_e$  is the eddy current loss,  $k_a$  is the coefficient of the anomalous eddy current loss,  $k_e$  is coefficient of the eddy current loss and  $B_m$  is the maximum magnetic flux density.

The  $k_a$  and  $k_e$  of different materials are different, The  $k_a$  and  $k_e$  for each sample are shown in Table 2. The maximum magnetic flux density of the integrated L-C-T is expressed by the following equations, as previously reported [26]:

$$B_m = B_{tra} + B_{ind} \quad (23)$$

$$B_{tra} = \frac{V_{in}}{2 A_c K_f n_{pri} f} \quad (24)$$

$$B_{ind} = \frac{L_k I_{pri}^2}{K_u A_p J} \quad (25)$$

where,  $B_{tra}$  is the maximum magnetic flux density of the transformer,  $B_{ind}$  is the maximum magnetic flux density of the inductor,  $J$  is the current density of the primary,  $A_c$  is the sectional area of the core center leg,  $A_p$  is the area product of the core,  $K_f$  is the coefficient of the square waveform,  $K_u$  is the occupied area of the core window.

### C. Winding losses

The general winding losses of the transformer can be expressed as:

$$\begin{aligned} P_{Cu} &= I_{pri}^2 R_{pri} + I_{sec}^2 R_{sec} \\ &= I_{pri}^2 \frac{\sigma l_{pri} n_{pri}}{A_{pri}} \left( \frac{R_{ac}}{R_{dc}} \right)_{pri} \\ &\quad + I_{sec}^2 \frac{\sigma l_{sec} n_{sec}}{A_{sec}} \left( \frac{R_{ac}}{R_{dc}} \right)_{sec} \end{aligned} \quad (26)$$

where,  $\sigma$  represents the conductivity of copper,  $l_{pri}$  is the average length of primary turns,  $l_{sec}$  is the average length of secondary turns,  $n_{sec}$  denotes the turns of the secondary windings,  $A_{pri}$  is the equivalent sectional area of the primary windings,  $A_{sec}$  is the equivalent sectional area of the secondary windings.

Generally, a Litz line is used to replace conventional line to eliminate the skin effect. Since the secondary of the novel integrated L-C-T is made of a Litz line, the skin effect of the secondary windings is not considered. In contrast, the skin

effect of the foil windings must be considered. Therefore, the AC factor of the secondary resistance  $(R_{ac}/R_{dc})_{sec} = 1$ , and the AC factor of primary resistance is as follows:

$$\left(\frac{R_{ac}}{R_{dc}}\right)_{pri} = y \left[ M(y) + \frac{2}{3}(n_{pri}^2 - 1)D(y) \right] \quad (27)$$

where,  $y$  denotes  $d_{foil}/\delta$ ,  $d_{foil}$  is the foil thickness (m),  $\delta$  is the skin depth at 20 kHz,  $M(y)$  is  $(\sinh(2y)+\sin(2y))/(\cosh(2y)-\cos(2y))$  and  $D(y)$  is  $(\sinh(y)-\sin(y))/(\cosh(y)+\cos(y))$ .

## VI. FEA VERIFICATIONS AND EXPERIMENTAL RESULTS

The main parameters of the novel integrated L-C-T are presented in Table 3. Accordingly, the FEA software (ANSYS Maxwell) is adopted to simulate the magnetic field of the novel integrated L-C-T, as shown in Fig. 8. The magnetic field distribution of the novel integrated L-C-T in chapter 2 is verified by FEA, and the leakage inductance of the novel integrated L-C-T is calculated, as shown in Fig.6. Moreover, in this paper, a prototype of the novel integrated L-C-T is used to verify the theory. The LCR meter is used to measure the leakage inductance and the interlayer capacitance. A comparison of the leakage inductances determined by the three different methods is presented in Fig.6, and a comparison of the interlayer capacitances determined by measurement and calculation is shown in Fig. 7. The comparisons in Fig.6 and Fig.7, revealed that the formulas of the leakage inductance and equivalent interlayer capacitance are accurate and suitable for the novel integrated L-C-T.

To ensure the proposed PSFB ZVS converter with integrated L-C-T to achieve soft-switching under light load, the leakage inductance of the novel integrated L-C-T is more than 20  $\mu$ H. Moreover, to ensure that the DC magnetic bias of novel integrated L-C-T is eliminated, the equivalent interlayer capacitance is about 37 $\mu$ F. As shown in Fig.6 and Fig.7, the prototype of the novel integrated L-C-T is designed to have 12 turns of  $n_{pri}$ , 4 turns of  $n_{s11}$ , 22 turns of  $n_{s12}$ . In addition, as shown in Fig.9, the comparison of the conventional separated components and the proposed integrated L-C-T indicates that the size and weight of the novel integrated L-C-T is half of the conventional components.

TABLE II  
FITTING COEFFICIENTS OF THE PROPOSED MODEL

Material	$K_a$	$K_c$
Nanocrystalline	$1.2 \cdot 10^{-5}$	$1.8 \cdot 10^{-7}$
Amorphous	$5.7 \cdot 10^{-5}$	$7.2 \cdot 10^{-7}$
6.5% silicon steel sheet	$1.1 \cdot 10^{-4}$	$4.4 \cdot 10^{-5}$
3% grain-oriented silicon steel sheet	$2.8 \cdot 10^{-4}$	$1.3 \cdot 10^{-5}$

TABLE III  
INTEGRATED L-C-T PARAMETERS

Parameter	Value
Primary winding	Foil
Secondary winding	Litz line
Dielectric material	Polyimide
Core material	Nanocrystal
Turns ratio( $a$ )	1.25
Area of center leg( $A_c$ )	25cm <sup>2</sup>
Area of side leg( $A_s$ )	12.5cm <sup>2</sup>
window height( $h_w$ )	10cm
window width along x axis( $b_w$ )	3cm
width along z axis( $l_w$ )	4cm
Mean turn length in primary( $l_a$ )	14cm
Mean turn length in secondary( $l_b$ )	20cm
Dielectric thickness	0.2mm
Insulator thickness( $h_i$ )	0.2mm

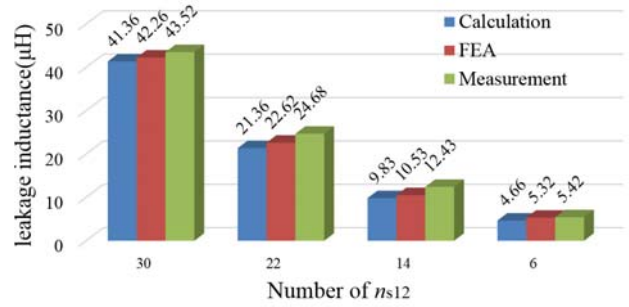


Fig. 6. Comparison of the leakage inductances by three different methods.

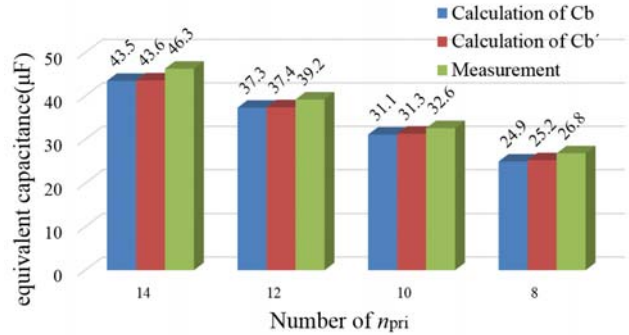


Fig. 7. Comparison of the equivalent capacitances by three methods.

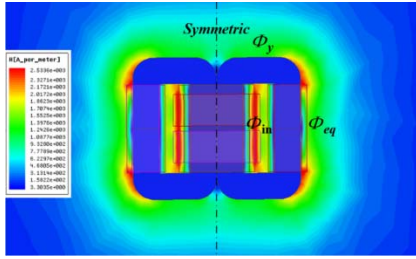


Fig. 8. Magnetic analysis of the novel integrated L-C-T

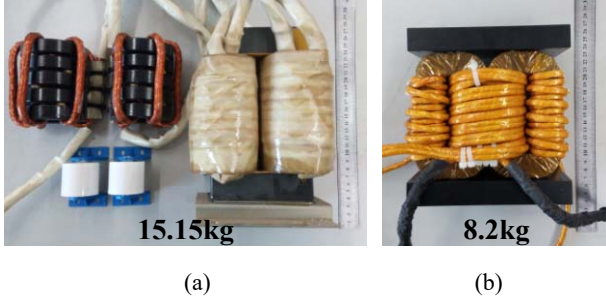


Fig. 9. Comparison of the conventional separated components and the novel integrated L-C-T. (a) Conventional separated components. (b) The novel integrated L-C-T.

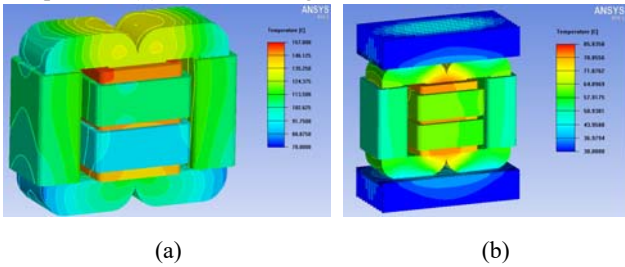


Fig. 10. Thermal analysis of the novel integrated L-C-T. (a) The novel integrated L-C-T with natural air cooling. (b) The novel integrated L-C-T with forced air cooling.

The losses of the novel integrated L-C-T are analyzed in chapter 5, then the FEA software (ANSYS Icepak) is used to simulate the temperature rise of the integrated L-C-T under high power (40 kW). As the temperature simulation of proposed L-C-T is shown in Fig. 10(a), the novel integrated L-C-T without the heat-sinks seriously overheats, the maximum temperature reaches 157°C (the point on the foil windings of the primary), the minimum temperature reaches 80°C (Litz line of the side column). To avoid the serious overheating, two heat-sinks (Aluminum alloy 6063) are installed at the upper and lower of novel integrated L-C-T. Moreover, natural air cooling is instead of the forced air cooling in the novel integrated L-C-T. The temperature rise of the novel integrated L-C-T with forced air cooling is shown in Fig. 10 (b). After the improvement, the maximum temperature is 85.8 °C, which is below the maximum permissible temperature for each material of the novel integrated L-C-T.

Finally, to verify the performance of the PSFB ZVS converter with the proposed L-C-T, a prototype with constant current, variable voltage and 40 kW power is developed, as

shown in Fig. 11. The prototype is implemented with following specifications: input voltage  $V_{in} = 340 - 420 V$ , output voltage  $V_{out} = 200 - 1000 V$ , output current  $I_{out} = 40 A$ , switching frequency  $f = 20 kHz$ , primary switches  $Q_1 - Q_4 = FF300R12KE4$ , transformer leakage inductance  $L_{lk} = 23.28 \mu H$ , high-frequency rectifiers  $DR_1 - DR_8 = DSEI 2x101$ , output inductor  $L_{out} = 1.6 mH$ , output capacitor  $C_{out} = 990 \mu F$ , and Fan = DB 1238B24H (12V, 21.6W, r/min = 6000). As the lagging switch is more difficult to reach ZVS than leading switch, the ZVS of lagging switch is implied the ZVS of the proposed converter. Fig. 13 shows the waveforms of lagging switch, where  $V_{CE}$  is the collector-emitter voltage of lagging switch,  $V_{GS}$  is the gate charge of lagging switch. As the lagging switch turns on after  $V_{CE}$  drops to zero, and turns off before  $V_{CE}$  increases from zero, the lagging switch reaches ZVS. Fig. 14(a) shows the waveforms of  $V_p$ ,  $I_p$  and  $V_{out1,2}$ , and  $V_{out1,2}$  is zero when  $V_p$  becomes 540 V. Apparently, the  $L_{lk}$  of proposed L-C-T resonates with the parallel capacitors ( $C_1 - C_4$ ) at that time.  $I_p$  flows through the freewheeling diodes of IGBTs and the primary winding of the L-C-T, and the voltage across lagging switches is clamped to zero. In addition,  $I_p$  is 50 A when  $V_p$  and  $V_{out1,2}$  become zero. In this interval,  $I_p$  flows through primary winding and the freewheeling diodes of IGBTs, and the leading switch can reach ZVS. There is a certain voltage distortion of the novel integrated L-C-T during the rising phase, but the proposed converter still achieved soft-switching at light-load. The waveforms of the proposed converter at heavy-load are shown in Fig. 14(b). The duty loss of the secondary voltage is within the acceptable range. Fig. 12 shows the power density comparisons of the proposed PSFB ZVS converter with the novel integrated L-C-T and conventional PSFB ZVS converter with separated magnetic components. Therefore, the novel integrated L-C-T can completely replace the separated components in the proposed PSFB ZVS converter, and further improves the power density of the converter.

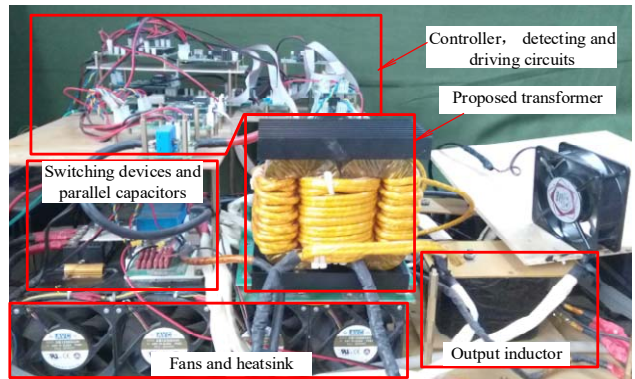


Fig. 11. The prototype of the proposed PSFB ZVS converter.

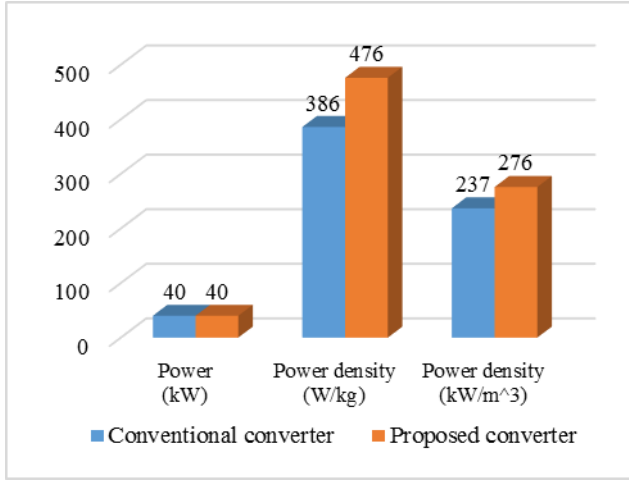


Fig. 12. The power density comparisons of conventional converter with separated magnetic components and proposed converter with the novel integrated L-C-T.

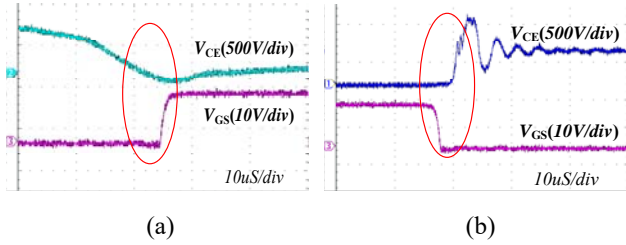


Fig. 13. Waveforms of lagging switch. (a)The turn-on waveforms. (b)The turn-off waveforms.

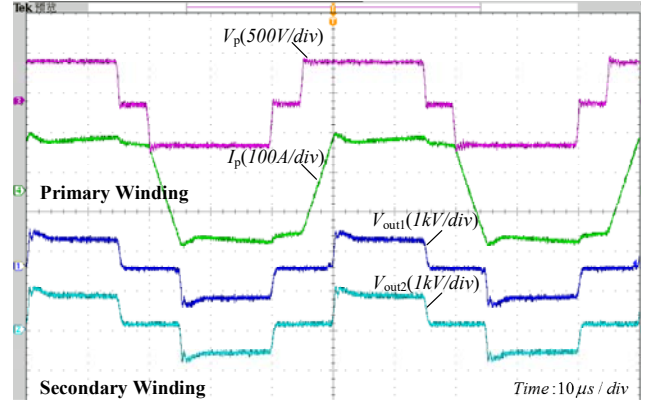
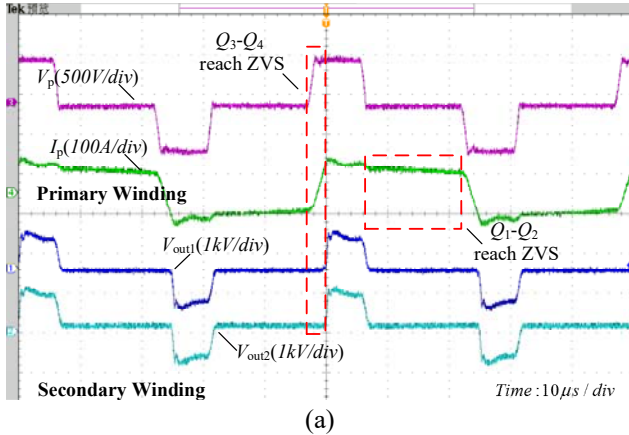


Fig. 14. Waveforms of the proposed IM transformer. (a) light-load condition. (b) 100% load condition.

## VII. CONCLUSIONS

A novel integrated L-C-T, which is suitable for the PSFB ZVS converter with high power and high voltage has been proposed and developed in paper. The calculation methods for the equivalent interlayer capacitance and leakage inductance of the novel integrated L-C-T are presented and verified by measurement and FEA. By simply setting the turns of the primary and secondary windings, the equivalent interlayer capacitance and leakage inductance of the proposed L-C-T can be easily designed. After the comparison with conventional transformer, the novel integrated L-C-T is found to decrease the size and weight by half. Additionally, through suitable thermal design, the temperature rise of the novel integrated L-C-T is limited to an acceptable range. Therefore, the novel integrated L-C-T in paper is very appropriate for the high power, high power density PSFB ZVS converter.

## ACKNOWLEDGEMENT

This work was supported by R&D of Instruments and Technologies for Deep Resources Prospecting (the National R&D Projects for Key Scientific Instruments), Grant No.ZDYZ2012-1-05.

## REFERENCES

- [1] G. N. B. Yadav, N. L. Narasamma, "An Active Soft Switched Phase-Shifted Full-Bridge DC-DC Converter: Analysis, Modeling, Design, and Implementation," *IEEE Trans. Power Electron.*, Vol. 29, No. 9, pp. 4538-4550, Sep. 2014.
- [2] S. H. Lee, C. Y. Park, J. M. Kwon et. al., "Hybrid-type full-bridge dc/dc converter with high efficiency," *IEEE Trans. Power Electron.*, Vol. 30, No. 8, pp.4156-4164, Aug. 2015.
- [3] K. Shi, D. Zhang, Z. Zhou et. al., "A novel phase-shift dual full-bridge converter with full soft-switching range and wide conversion range," *IEEE Trans. Power Electron.*, Vol. 31, No.11, pp. 7747-7760, Nov. 2016.
- [4] Y. Jiang, Z. Chen, J. Pan, "Zero-voltage switching phase



- shift full-bridge step-up converter with integrated magnetic structure,” *IET Power Electronics*, Vol. 3, No. 5, pp.732-739, Dec. 2009.
- [5] Y. Jang, M. M. Jovanović, Y. M. Chang, “A new zvs-pwm full-bridge converter,” *IEEE Trans. Power Electron.*, Vol. 18, No. 5, pp. 232-239, 2002.
- [6] K. U. Member, “A generalized method for lagrangian modeling of power conversion circuit with integrated magnetic components,” *IEEJ Trans. Electr. Electron.*, Vol. 7, No. S1, pp. 146-152, 2012.
- [7] K. Umetani, S. Arimura, T. Hirano et. al., “Evaluation of the Lagrangian method for deriving equivalent circuits of integrated magnetic components: A case study using the integrated winding coupled inductor,” *IEEE Trans. Ind. Appl.*, Vol. 51, No. 1, pp.547-555. Jan/Feb. 2015.
- [8] M. Pahlevani, S. Eren, A. Bakhshai et. al., “A series-parallel current-driven full-bridge dc/dc converter,” *IEEE Trans. Power Electron.*, Vol. 31, No. 2, pp. 1275-1293, Feb. 2016.
- [9] N. Zhu, J. D. van Wyk, F. Wang, “Design of integrated parallel resonant transformers,” in *IEEE Power Electronics Specialists Conference*, pp. 1787-1792, 2005.
- [10] J. T. Strydom, J. D. van Wyk, J. A. Ferreira, “Some limits of integrated L-C-T modules for resonant converters at 1MHz,” *IEEE Trans. Ind. Appl.*, Vol. 37, No. 3, pp. 820-828, May/June. 2001.
- [11] J. T. Strydom, “Electromagnetic design of integrated resonator-transformers,” PhD. Thesis, Rand Afrikaans University, 2001.
- [12] W. Liu, “Alternative structures for integrated electromagnetic passives,” PhD. Thesis, Virginia Tech., 2006.
- [13] Z. Ouyang, J. Zhang, W. G. Hurley, “Calculation of leakage inductance for high-frequency transformers,” *IEEE Trans. Power Electron.*, Vol. 30, No. 10, pp. 5769-5775, Oct. 2015.
- [14] M. A. Bahmani, T. Thiringer, “Accurate evaluation of leakage inductance in high-frequency transformers using an improved frequency-dependent expression,” *IEEE Trans. Power Electron.*, Vol. 30, No. 10, pp. 5738-5745, Oct. 2015.
- [15] R. Doebbelin, C. Teichert, M. Benecke et. al., “Computerized calculation of leakage inductance values of transformers,” *Piers Online*, Vol. 5, No. 8, pp. 721-726, Aug. 2009.
- [16] R. Chen, J. T. Strydom, J. D. van Wyk, “Design of planar integrated passive module for zero-voltage-switched asymmetrical half-bridge PWM converter,” *IEEE Trans. on Ind. Appl.*, Vol. 39, No. 6, pp. 1648-1655, Nov/Dec. 2003.
- [17] I. W. Hofsjager, J. A. Ferreira, J. D. van Wyk, “Design and analysis of planar integrated LCT components for converters,” *IEEE Trans. Power Electron.*, Vol. 15, No. 6, pp. 1221-1227, Nov. 2000.
- [18] M. C. Smit, J. A. Ferreira, J. D. Van Wyk et. al., “An ultrasonic series resonant converter with integrated LCT,” *IEEE Trans. Power Electron.*, Vol. 10, No. 1, pp. 25-31, Jan. 1995.
- [19] P. A. J. van Rensburg, J. D. van Wyk, J. A. Ferreira, “Design, prototyping and assessment of a 3 kW integrated LCT component for deployment in various resonant converters,” *IET Power Electron.*, Vol. 2, No. 5, pp. 535-544. Aug. 2008.
- [20] Y. Lembeye, P. Goubier, J. P. Ferrieux, “Integrated planar l-c-t component: design, characterization and experimental efficiency analysis,” *IEEE Trans. Power Electron.*, Vol. 20, No. 3, pp. 593-599, May. 2005.
- [21] L. Dalessandro, F. S. Cavalcante, J. W. Kolar, “Self-capacitance of high-voltage transformers,” *IEEE Trans. Power Electron.*, Vol. 22, No. 5: pp.2081-2092, Sep. 2007.
- [22] J. Biela, J. W. Kolar, “Using transformer parasitics for resonant converters-A review of the calculation of the stray capacitance of transformers,” *IEEE Trans. Ind. Appl.*, Vol. 44, No. 1, pp.223-233, Jan. 2008.
- [23] A. Pressman, “Switching power supply design,” McGraw-Hill, 2009, Chap.3.
- [24] V. K. Lebedev, “Calculation of the short-circuit resistance of welding transformers with yoke leakage (russ.),” *Automatic Welding*, Vol. 11, No. 4, pp. 37-44, 1958.
- [25] R. Doebbelin, M. Benecke, A. Lindemann, “Calculation of leakage inductance of core-type transformers for power electronic circuits,” in *Proc. Power Electronics and Motion Control Conf.*, pp. 1280-1286, 2008.
- [26] C. W. T. Mcllyman, “Transformer and inductor design handbook,” M. Dekker, 1978, Chap.7/8.



**Jia-shen Tian** was born in Beijing, China, in 1990. He received his B.E. from the College of Electrical and Electronic Engineering, North China Institute of Science & Technology, Hebei, China in 2012, and he received his M.E. from the Faculty of Information, Beijing University of Technology, Beijing, China in 2015, respectively. He is currently working towards his Ph.D. in the Faculty of Information, Beijing University of Technology, Beijing, China. He is participating in research dealing with quality control of electrical equipment, electric tests and tests on the electromagnetic compatibility of electrical and electronic equipment. His current research interests include modeling and control of switching power supplies, magnetic components, system optimization concerning electromagnetic fields and high voltages.



**Junxia Gao** was born in Tianjin, China, in 1978. She received her B.E. from the College Information Engineering, Taiyuan University of Technology, Taiyuan, China in 2001, and her M.E. from the Faculty of Information, Beijing University of Technology, Beijing, China in 2004, respectively. Since 2004, she has been a senior lecturer in the Faculty of information, Beijing University of Technology, Beijing, China. Her current research interests include power electronics, electromagnetic field and nondestructive examination.



**Yi-ming Zhang** was born in Hubei, China, in 1964. He received his B.E. from the School of Electronic, Information and Electrical Engineering, Shanghai Jiao Tong University, Shanghai, China, in 1988, and his M.E. from the School of Electrical Engineering and Automation, Harbin Institute of Technology, Harbin, China in 1992. From 2000 to 2007, he was a Senior Researcher in the Institute of Electrical Engineering, Chinese Academy of Sciences,

Beijing, China. Since 2008, he has been an Professor in the College of Electronic Information and Control Engineering, Beijing University of Technology, Beijing, China. His current research interests include intelligent power management, motor speed control, servo drivers and motor energy conservation.